The Journal of Adhesion, 92:194–213, 2016

ISSN: 0021-8464 print/1545-5823 online
DOI: 10.1080/00218464.2015.1018512

Adhesion Behavior of a Grating at a Single Location by Using an AFM Flat Tip Under Different Conditions

TIANMAO LAI, SHENGGUANG ZHU, and PING HUANG

School of Mechanical and Automotive Engineering, South China University of Technology, Guangzhou, Guangdong, China

Adhesion forces were determined by recording force–displacement curves using a flat tip with an atomic force microscope. The outcomes show that the adhesion behavior at a single location depends largely on contact geometry, surface topography, instrumental parameters, and the environment. Moreover, these factors are mutually coupled with each other to determine the final adhesion force. A special surface structure will lead to special adhesion behaviors by repetitive measurements. The adhesion forces are grouped into several levels. In dry nitrogen (with charges removal), the adhesion force in each level first increases and then decreases slightly. In dry nitrogen and under ambient conditions, the adhesion force in different levels increases with measurement number, and jumps between different levels. The increasing trend was ascribed to the charge accumulation and the increased size of the capillary meniscus, respectively. The charges will increase only after contact and separation and have an additive effect. When the charges are saturated, the adhesion force becomes stable. Some special adhesion behaviors are also observed in the experiments. The fluctuation behaviors of adhesion in a single cluster under different conditions are different, which was attributed to the dominant force and the environment.

Received 24 October 2014; in final form 9 February 2015.

Address correspondence to Tianmao Lai, School of Mechanical and Automotive Engineering, South China University of Technology, Wushan Road 381, Tianhe District, Guangzhou, Guangdong 510640, China. E-mail: laitianmao@163.com

Color versions of one or more of the figures in the article can be found online at www.tandfonline.com/gadh.

KEYWORDS Atomic force microscope; Contact electrification; Dry adhesion; Force–displacement curve; Patterned surfaces

1. INTRODUCTION

The adhesion property between two solid surfaces is of major interest in many scientific and industrial fields. With the rapid development of micro–nano devices and instruments, such as micro-/nano-electromechanical systems (MEMS/NEMS) and magnetic storage devices, this kind of adhesion becomes more and more important. Small-scale mechanical systems are more influenced by surface effects rather than inertia effects, since they have high surface-area-to-volume ratios. The adhesion force is the dominant factor of the failures of MEMS/NEMS in manufacture and in use [1, 2]. Therefore, it is urgent to develop a sophisticated understanding of the adhesion behavior between two solid surfaces.

Generally, the adhesion force is a combination of the electrostatic force, the van der Waals (vdW) force, the capillary force and so on [3]. Under different conditions, the dominant contributions of adhesion may be different. Under ambient conditions, the capillary force is the dominant force. And it is always present due to capillary condensation and the adsorption of thin water films on surfaces. In dry gaseous environments, the capillary force will disappear, and the vdW force and electrostatic forces may become the dominant forces. In particular, the electrostatic force can be large on insulators, since charge dissipation is ineffective at low humidity. Under distilled water, in general, there is no capillary force and electrostatic force. The significant contribution is the vdW force.

In order to understand the adhesion force, measuring the adhesion force is required in advance. There are numerous apparatuses to measure adhesion at the microscopic scale, such as surface force apparatus (SFA), interfacial force microscope (IFM), and atomic force microscopy (AFM), and so on. Among them, the AFM has been widely used in the adhesion force measurement. It provides a simple and accurate way to determine adhesion forces with high spatial resolution. It is possible to measure the adhesion force between any types of surfaces in any environment. The adhesion force between the tip and sample is determined by recording a force–displacement curve. The force–displacement curve is obtained by monitoring the deflection of a cantilever as the tip approaches and retracts from the sample.

When obtaining adhesion forces by the AFM, the tip shape is a very important factor. A sharp tip widely used usually has a parabolic shape with an end radius varying from 10 to 100 nm. However, sharp tips wear easily. This is a serious disadvantage, since wear will result in the variation of the contact area between the tip and sample [4]. Therefore, the number of measurement by the sharp tip is always small. The shortcoming can be

overcome by the introduction of colloid probe technique [5]. A spherical particle can be attached to the end of a cantilever. The accessible range of particle size is typically limited to a range between 1 and 50 μm. This kind of probe has become a well-established tool for studying adhesion due to its defined geometric shape and wear resistance. A probe tip with a large and flat cylindrical end can not only overcome the shortcoming, but also be used to mimic a flat surface. This kind of tip has been used in a few experiments to study adhesion forces. For example, Ando [6] studied the adhesion forces between a Ni tip with a 0.1 μm^2 flat area and a flat Si substrate. Ferreira *et al.* [7] used flat probe tips with diameters of 1 and 3 μm to measure the adhesion force of some flat and smooth surfaces. Çolak *et al.* [8] used a flat tip with a diameter of 2 μm to measure the adhesion forces of a smooth and chemically etched Si (100) surface.

It was well known that many factors can influence adhesion, such as surface roughness [9], temperature [10], humidity [11], and experimental parameters [7, 12]. Some factors are well-studied. However, there are only a few studies concerning the influence of repetitive measurements at the same location. Repetitive measurements at a single location are usually used to examine the reproducibility of the adhesion measurements. Therefore, the numbers of measurement are usually relatively small. For example, Ibrahim *et al.* [13] used a lactose particle (6 μm) to measure the adhesion force 50 times at a single location on a gelatin capsule surface at 50% relative humidity (RH) by an AFM. They reported that there does not appear to be any appreciable change in the adhesion force with measurement number. Tormoen and Drelich [14] used a spherical polystyrene tip (diameter 10 ± 1 μm) to record 100 force–displacement curves sequentially at a single location on a smooth silicon wafer in a sub-5% RH environment using an AFM. They found that the adhesion force shows no characteristic trend, and the scatter in the data for measurements is about 10%. From these, they concluded that the probe did not undergo any plastic deformation under the experimental conditions. Çolak *et al.* [12] used a silicon flat tip (diameter ~0.9 μm) to collect 20 force–displacement curves consecutively at the same location on a Si (001) wafer at different normal loads at 0% and 40% RH using an AFM. The outcomes showed that there is no tendency for either an increase or a decrease between individual measurements within the experimental error. In a recent work of Lai and Huang [15], consecutive measurements (128 or 256 times) at a single location between a flat tip (diameter ~1.73 μm) and some samples were carried out under ambient conditions, in dry nitrogen and under distilled water. The outcome shows that numerous measurements at the same location will not affect adhesion greatly if the surface is smooth enough, but may lead to increased adhesion due to the plastic deformation or damage of the asperities. It can be seen that the numbers of measurement in these studies are all relatively small. Several questions can be addressed. The first one is what will happen when increasing the measurement number.

The second is whether a special surface structure will lead to special adhesion behavior by repetitive measurements. Therefore, the adhesion behavior at a single location is not yet conclusive, and a detail investigation is still necessary.

In this paper, the adhesion behaviors of a calibration grating were studied in dry nitrogen and under ambient conditions. The adhesion forces were determined by recording force–displacement curves using a flat tip with an AFM. The topographical characterization of the sample was analyzed by the AFM image. Several locations on the sample surface were selected to collect hundreds of force–displacement curves consecutively by the tip under different conditions. The relation of adhesion force and sequential measurement number was studied. Adhesion behaviors were compared for different conditions. The reasons why we obtain these adhesion behaviors were discussed. The results of this paper can provide a reference to the adhesion experiments of an AFM.

2. EXPERIMENTAL

The sample used was a holographic grating (Changchun Hengyu Photoelectric Technology, Changchun, China). It is made of optical glass and is electrically insulated. The grating contains a regular array of sinusoidal-like ridges. The ridges of the grating have a uniform configuration and are isolated to each other. Before the experiments, the sample was ultrasonically cleaned in an alcohol solution for 15 min, and then ultrasonically cleaned in distilled water for 15 min.

The measurements of adhesion forces (pull-off forces) were performed by using an AFM (Being Nano-Instruments CSPM-4000, Guangzhou, China) of beam deflection type. The microscope was operated under ambient conditions (temperature 20°C ± 1°C, relative humidity is 70% ± 3%) and in a nitrogen-filled glove box (Etelux Lab2000, Etelux Inert Gas System Company Limited, Beijing, China) where the temperature was 26°C ± 1°C and the water content was less than 0.1 ppm.

A probe with a flat tip was used to measure adhesion forces in this study. The probe is a single crystalline silicon probe (PL2-CONTR, Nanosensors, Neuchatel, Switzerland). Figure 1 shows the tip shape after the experiments. The figure was obtained by using a scanning electron microscopy (SEM, Zeiss MERLIN Field Emission SEM, Carl Zeiss NTS GmbH, Oberkochen, Germany). An intentionally blunt tip with a well-defined circular end-face is located at the free end of a rectangular cantilever. The flat tip is formed by focused ion beam milling and has a ~1.73 μm diameter contact area. The tip did not show the sign of wear comparing with the shape before experiments. However, the tip was contaminated by some garbage and the dust after experiments. The spring constant of the cantilever was determined

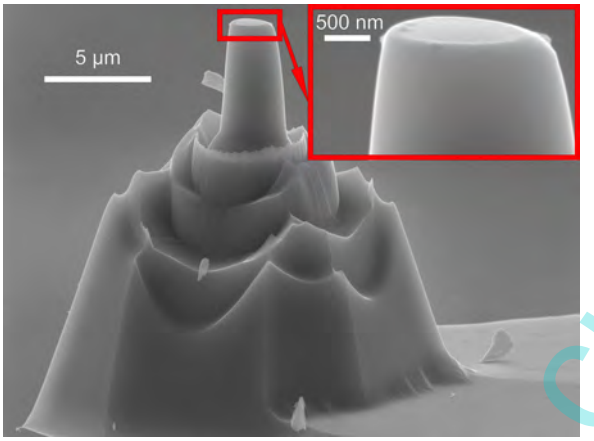

FIGURE 1 Scanning electron microscope image of the flat tip.

with the thermal tune method by using an AFM (MFP-3D Classic, Asylum Research, Santa Barbara, CA, USA) [16]. The spring constant of the cantilever was 0.132 N/m.

In the AFM, adhesion force measurements are performed by recording force–displacement curves. A typical force–displacement curve is shown in Fig. 2. The approaching and retracting process is from Point A to Point H. (A) When the sample is initially far away from the tip, the voltage of the photodetector is zero, and no measurable interaction is detected. This segment is regarded as a zero line. (B) Upon approaching the surface, the end of the cantilever will bend downward (upward) due to the attractive (repulsive) forces. (C) If the short-range attractive force gradient of the tip-sample interaction exceeds the normal spring constant of the cantilever, the tip will snap into contact with the sample (D). The tip and sample will keep in contact after that. As the sample moves up continuously, the curve eventually crosses the zero line (E). At this point, the voltage of the photodetector is zero again. (F) The tip-sample interaction continues to increase

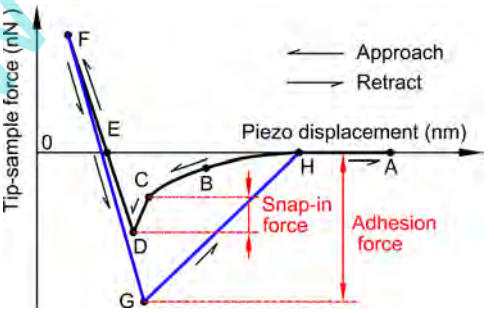

FIGURE 2 A schematic of a typical force–displacement curve with highlights of the various stages (A–H) as the tip is brought into and out of contact with the sample at a fixed location.

as the sample moves upward, until a predetermined maximum normal load is reached. The retraction of the sample will result in the decrease of the interaction. With the withdrawal of the sample, the tip keeps in contact with the sample because of the adhesion force. (G) When the normal spring constant overcomes the attractive force gradient, the cantilever snaps back to its original undeflected position. The segment FG is referred to the contact line of the retraction curve. If the tip senses the attractive force, the cantilever will go back to its original starting position slowly (not shown in Fig. 2). Figure 2 also shows the snap-in force and the adhesion force. In the experiments here, hundreds of force–displacement curves were collected consecutively at a single location on the sample. Then the relation of adhesion force and measurement number was studied.

In dry gaseous environments, the vdW force and electrostatic force become the dominant forces. There will be many static charges on an insulating sample, since the charge dissipation is ineffective at low humidity. When needed, an anti-static copper bar (SY-504, Shenzhen Shengyuan Anti-static Corporation, Guangdong, China) can be applied over the substrate to eliminate any static charge buildup. It is an ion generating device and is employed to establish a field of ionized air in which the charges on the substrate are neutralized.

Contact angle measurements were conducted on OCA 40 Micro (Data-Physics Instruments GmbH, Filderstadt, Germany). Three probe liquids with different surface tensions and surface tension components (diiodomethane, glycerol, and distilled water) were used for these measurements. The contact angles were measured for at least five liquid drops having a base diameter from 4 to 6 mm. The pollution of different liquids and the mutual influences between measurements should be avoided. Therefore, after each measurement, the sample was ultrasonically cleaned in an alcohol solution for 1 min, followed by ultrasonically cleaning in the distilled water for 1 min, and then drying. All measurements were conducted at room temperature, 27°C ± 1°C.

3. RESULTS AND DISCUSSION

3.1. Sample Surface Characterization

The surface topographies of the sample has been determined from an imaged area of 5 μm × 5 μm which is the representative of the sample, as shown in Fig. 3(a). A sharp probe (ContAl, Budget Sensors, Innovative Solutions Bulgaria Limited, Sofia, Bulgaria) with tip radius less than 10 nm was used to measure the surface topographies by contact mode. The surface roughness is quantified using root-mean-square (RMS) roughness R_q. The parameter is defined by

$$R_q = \sqrt{\frac{1}{n}\left[\sum_{i=1}^{n}(z_i - z_{ave})^2\right]}, \tag{1}$$

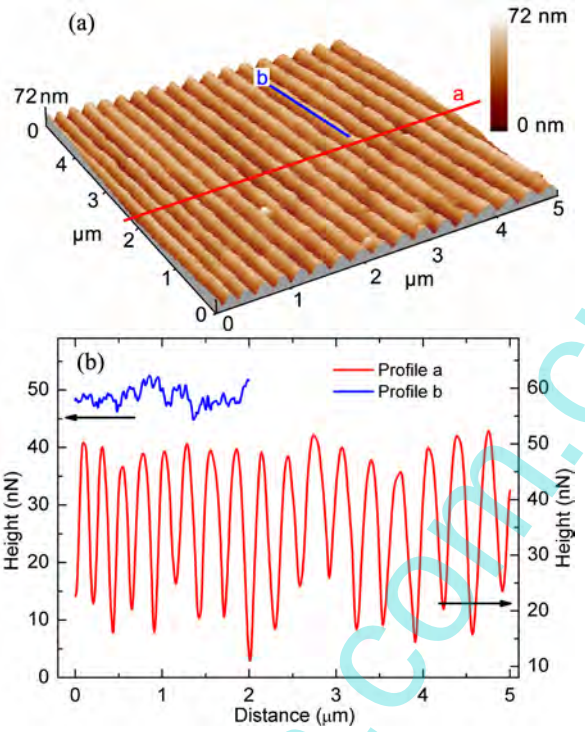

FIGURE 3 (a) 5 μm × 5 μm AFM contact mode image of the substrate grid. Two straight lines parallel and perpendicular to the ridge direction are used to create the profiles. (b) 5 μm cross-sectional profile perpendicular to the ridge, and 2 μm cross-sectional profile of the ridge taken along the ridge side wall.

where z_i is the topographic height at point i, n is the number of points measured within the area, z_{ave} is the average value of topographic heights within the area, $z_{ave} = \left(\sum_{i=1}^{n} z_i\right)/n$. The RMS roughness was determined for the image presented in Fig. 3(a) and found to be ~10.8 nm. Two straight lines parallel and perpendicular to the ridge direction shown in Fig. 3(a) are used to create the profiles. The cross-sectional profiles are shown in Fig. 3(b). The peak-to-peak distance was measured from the cross-sectional profile perpendicular to the ridges. From Fig. 3(b), the distance spanning 16 ridge peaks was measured to be 4.662 μm, which gives an average peak-to-peak distance of ~291 nm. The cross-sectional profile taken along the ridge side wall is used to better characterize irregularities of the surface. It can be seen from the profile that the height of nanoscale irregularities varied from less than 2 nm to about 5 nm. The RMS roughness of this profile is ~1.52 nm. These asperities on the sidewall or top of the ridges can significantly alter the tip–substrate contact area during adhesion force measurements.

The surface free energy of the sample was calculated by the Oss-Chaudhury-Good (vOCG) theory [17, 18]. The contact angle with water is $74.0° \pm 2.7°$, and the surface free energy is ~38.8 mJm^{-2}.

3.2. Adhesion Forces Measured by the Flat Tip

When using the flat tip, great care should be taken to the alignment between the flat surface of the tip and the sample [8]. To make sure that the tip makes contact with the sample before any components (such as the cantilever chip or the clip of the cantilever holder), the cantilever is tilted by ~11° in the AFM we used. After the tip jumping into contact, the voltage of the photodetector will be zero again as the sample moves up continuously (Point E in Fig. 2). After that, the cantilever will bend upward with the increase of the interaction until the maximum applied load is reached. Figure 4 shows the possible contact scenarios between the flat tip and a flat sample in this process (the sample here is assumed to be flat). Since the tip surface is parallel with the cantilever, the surface of the tip will be tilted by ~11° with the flat sample at first, as shown in Fig. 4(a). The distance between the rear point B and the sample (the largest clearance) is ~0.33 μm. In our experiments of the flat tip, the maximum applied load is ~390 nN. That means the piezo displacement between Point E and Point F (shown in Fig. 2) is ~2.8 μm, which is much larger than the largest clearance. Therefore, the tip must have experienced the scenario shown in Fig. 4(b). That is, the flat surface of the tip is parallel to the sample. However, the scenario shown in Fig. 4(c) may not happen, due to the adhesion force between the tip and the sample. It is not a big deal that the front end of the tip becomes out of contact with the sample, since the tip will experience the parallel contact [shown in Fig. 4(b)] once again with the retraction of the sample. It should be noted that the flat tip may not experience the parallel contact with the sample, if the maximum applied load is small. That is why the maximum applied load used here is large. When using the flat tip, the loading rate is ~520 nNs^{-1}, the retraction velocity of the tip is ~3.85 μms^{-1} and the dwell-in time is 0 s.

In dry nitrogen, a location (Location 1) was selected on the sample surface to collect 1024 force–displacement curves consecutively. The relation of adhesion force and measurement number is shown in Fig. 5(a). As can be seen from Fig. 5(a), the data of adhesion force are grouped into several clusters. When the measurement number is lower than 550, the adhesion force

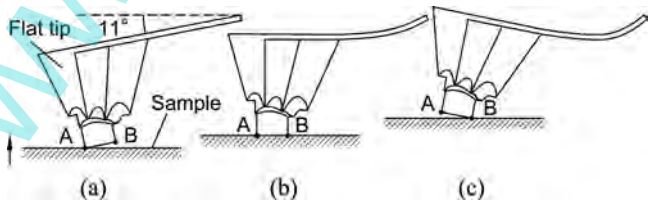

FIGURE 4 Schematics of contact scenarios between the flat tip and a flat sample: (a) only the front end of the tip is contacted with the sample, and the voltage of the photodetector is zero, (b) the end-face of the tip is parallel with the sample, and (c) only the rear end of the tip is contacted with the sample.

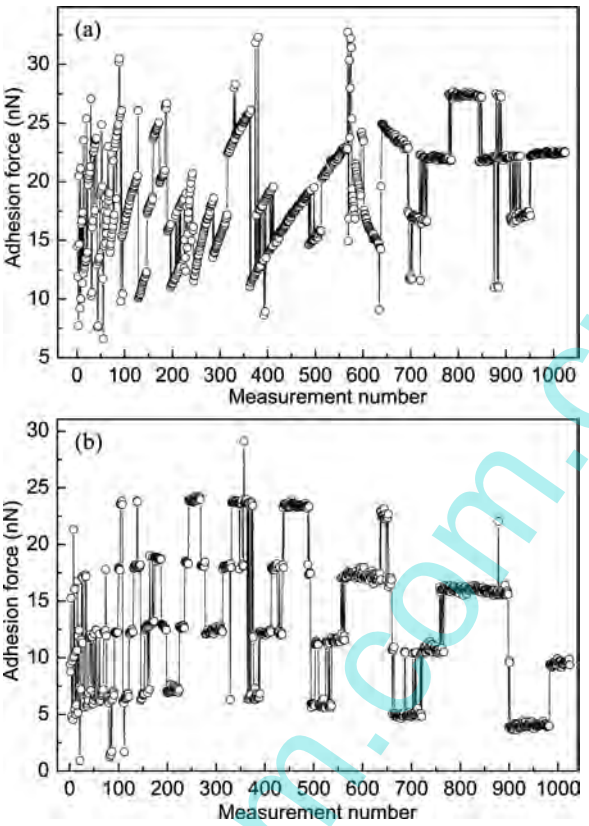

FIGURE 5 Adhesion forces versus sequential measurement number using the flat tip (a) at Location 1 in dry nitrogen and (b) at Location 2 in dry nitrogen with static charges removal.

continues to increase in each cluster. The adhesion force jumps to the other cluster at the end of a cluster. The adhesion force also jumps between clusters, especially when the number is lower than 100, and around 400. The adhesion force continues to decrease in each cluster between 550 and 700. Between 700 and 1024, the adhesion forces are divided into 4 levels, and remain stable in each level.

In order to study the behavior of adhesion with static charges removal, the anti-static copper bar was placed ~100 mm above the tip. The experiment was carried out after about 20 min. The relation of adhesion force and measurement number is shown in Fig. 5(b). The data of adhesion force are grouped into 6 levels. Only a few data points are in the minimum and maximum levels. The adhesion forces in separate levels seem to increase manifold (~0, ~6, ~12, ~18, ~24, and ~30 nN respectively). The adhesion force jumps frequently between levels, especially when the number is lower than 100. From the 4 levels in the middle, the adhesion first increases and then decreases slightly with measurement number.

From the above description and Fig. 5, the behaviors of the adhesion force under both situations are complicated. Following, the change trends of the adhesion force will be discussed firstly. Then the reason why the data of adhesion force are grouped into different clusters or levels will be analyzed. For convenience, some force–displacement curves are chosen from the curves collected on Locations 1 and 2. Figure 6 shows the approach segments (jumping into contact) of the curves. Upon approaching the surface, the end of the cantilever bends downward due to the attractive force, even when the tip is far away from the sample. The feature is caused by the long-range electrostatic force. As can be seen from Fig. 6(a), this feature becomes more and more clear with the increase of the measurement number. That means the force exerted on the tip increases with measurement number when the tip does not contact with the sample. When the number is lower than 80, the snap-in force also increases with the measurement number. Therefore, the continuous increasing trend of the adhesion force in each cluster in Fig. 5 (a) can be ascribed to the accumulation of electrostatic charges.

In our experiments, the tip is a semiconductor and the sample is an insulator. After coming into contact and then separating with each other, both the tip and the sample acquire electric charges. This is a phenomenon of contact electrification (CE). Although the research of CE involving insulators is dated back to Thales of Miletus, there is still a controversy regarding the mechanism of charge separation across the interface [19]. There are three ways for the transfer of electric charges: electron transfer, ion transfer, and transfer of charged material fragments [20]. Each of these may play a part in the charge transfer. The transfer mechanism will not be considered here. What we are concerned is the electrostatic interactions between the tip and the sample, caused by transferred charges across the interface *via* CE. Before the experiments, both surfaces of the tip and the sample may be

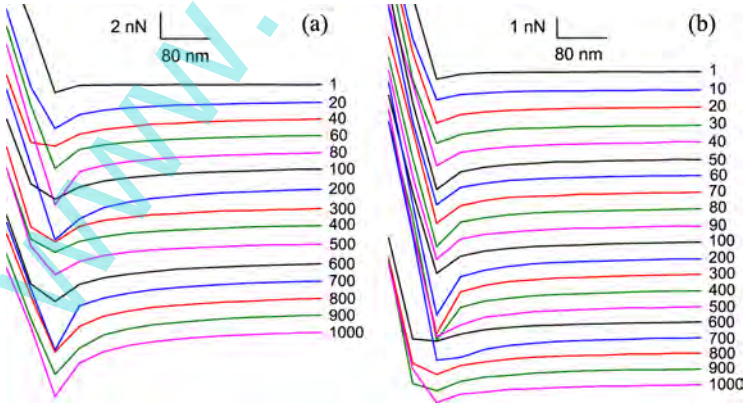

FIGURE 6 Lines of the approach segments of force–displacement curves: (a) at Location 1 in dry nitrogen and (b) at Location 2 in dry nitrogen with static charges removal. The measurement numbers are marked on the right side of the curves.

electrically neutral. Or there are only a few charges on the surfaces. This can be seen from the zero line of the first force–displacement curve, as shown in Fig. 6(a). The line can nearly be regarded as a straight line since no long-range electrostatic force was sensed by the tip. After the tip and the sample come into contact by a normal load, electric charges will transfer across the interface, as implied by the CE theory. When the tip jumps off contact with the sample, the charges transferred upon contact will be separated during the interfacial fracture process. Then one of the materials will become positively charged, while the other negatively charged. This leads to the formation of the electrostatic interaction between the surfaces. For the sample (insulator), electric charges accumulated *via* CE will be trapped at the surface, since the charges cannot efficiently transfer into the matrix [21, 22]. Therefore, the sample is prone to get highly charged. Also, in dry nitrogen, the water content is less than 0.1 ppm, and the conductivity of the gas is relatively weak. Therefore, it is difficult for the charge build-up to dissipate gradually and the ability of holding charge of the materials increases. It also should be noted that some previous obtained charges will be neutralized after contact. However, the flat tip cannot probe the grooves between the ridges and the valleys between the asperities to neutralize the charges there. All of these lead to the accumulation of charges.

After the tip jumps off contact with the sample, one of the surfaces will be positively charged, while the other negatively charged. When collecting the next curve, the tip will be brought close the sample once again. The long-range electrostatic force exerted on the tip will bend the cantilever downward due to the attractive force. The electrostatic force between two point charges (q_1 and q_2) with the distance d can be expressed by Coulomb's inverse-square law, $F_{el} = q_1 q_2 / (4\pi\varepsilon_0 d^2)$, where ε_0 is the permittivity of free space. With the decrease of the distance, the interaction force will increase. For two charged dielectric materials, the interaction force should be calculated by using the image charge method and numerical method [23–25]. After calculation, the dependence of the force on the distance is the same. That is, the force will increase with the decrease of the distance. As can be seen from Fig. 6(a), the attractive force becomes larger when the tip comes closer to the sample. When the interaction force gradient exceeds the spring constant of the cantilever, the tip eventually jumps into contact with the sample.

During the separation of the surfaces, the charges newly obtained and the residual charges obtained before would ultimately build up an electric field between the two surfaces. It is worthwhile mentioned that conventional contact mechanics theories, cannot predict the adhesion properties of charged surfaces. By using the model of parallel plate capacitors, the electrostatic force developed can simply be approximated by [26–28]

$$F_{el} = \frac{A\sigma^2}{2\varepsilon_0}, \tag{2}$$

where σ is the surface charge density (assumed equal on both surfaces), A is the real contact area. As mentioned above, charges accumulated *via* CE will be trapped at the surface, and are difficult to be dissipated or neutralized. Therefore, after the tip touches and then jumps off the sample so many times, the charges on the surface will be accumulated gradually. That means the surface charge density will increase with the measurement number. If we assume that the real contact areas are the same, this eventually leads to the increase of the electrostatic force, as can be seen from Equation (2). The electrostatic force is one part of the adhesion force (the other is the vdW force), and this explains the increase trend in each cluster shown in Fig. 5(a).

However, the surface charge density cannot always be increased. That is, the magnitude of the net charge on a surface caused by CE has an upper limit. There are a few factors that determine the upper limit of the surface charge density. First, the charge density on a surface will become so high by consecutive contacts that the voltage can reach the threshold value for the dielectric breakdown of air and the charges are conducted through the air [29]. Second, the transfer of charges must move against the force of a repelling electric field created by the previous charges [30]. It is energetically unfavorable. Finally, the magnitude of the charge on a surface could also be limited by a finite number of states or charge carriers, and the leakage of charge to a grounded surface [20]. Therefore, static charges will be saturated in a position due to the upper limit of the surface charge density, leading to stable adhesion forces. This explains that the adhesion force of each level remains stable when the measurement number is between 700 and 1024, as shown in Fig. 5(a).

The complication of CE is shown not only by the upper limit of the surface charge density, but also by the non-uniformity of charges [31] and the polarity reversal [32]. As implied by the CE theory, after the separation of two surfaces, one will become positively charged, while the other negatively charged. However, as suggested by the experiments of Baytekin *et al.* [31], the respective surfaces may have both positive and negative regions on the nanoscale. That means, the net charge on a surface represents a balance between the contributions from unlike charged regions. Therefore, the average net surface charge density may be decreased with the shift in the relative contributions of positive and negative regions. This may be one of the reasons why the adhesion force continues to decrease in each cluster between 550 and 700, as shown in Fig. 5(a). The polarity reversal is also demonstrated by the experiments of Baytekin *et al.* [32]. In their experiments, Teflon beads were contacted and separated consecutively with a polystyrene dish by shaking. Within a minute, the Teflon beads were negatively charged. However, they became positively charged after a few minutes. This polarity reversal was attributed to the material transfer. That is, nanoscale patches of material on one surface are torn off and transferred onto the other surface. Baytekin *et al.* pointed out that this material transfer process depends on the

mechanical properties of the material, such as the material hardness and cohesive energy. In our experiments, the material transfer may happen after so many contacts between the tip and sample. This may be the main reason why the adhesion force continues to decrease in each cluster between 550 and 700, as shown in Fig. 5(a). In Fig. 5(a), the increasing, decreasing and stable trends of the clusters of adhesion force are shown in a series of touches. That means, the phenomenon of CE is really complicated. Based on the results of Baytekin *et al.* [32], Lacks concluded that perhaps contact charging may never be predictable, since the material transfer can never be avoided in contact charging experiments [33].

It should be noted that, if the plastic deformation of nano-irregularities on the ridges happens, the contact area will increase and eventually the adhesion will increase with the measurement number. However, based on the results with static charges removal [shown in Fig. 5(b)], the increase trend shown in Fig. 5(a) should not be attributed to the plastic deformation. That is, if the plastic deformation happens by repetitive contacts, we will not get the decreasing trend of the adhesion force shown in Fig. 5(b).

As shown in Fig. 6(b), with static charges removal, the clearness of the bending feature (caused by the long-range electrostatic force) increases slightly with the increase of the measurement number, when the number is lower than 100. Also, when the number is lower than 100, the snap-in force also increases with the measurement number. These are in accordance with the increasing trend of the adhesion force for the 4 levels in the middle, as shown in Fig. 5(b). Therefore, it is reasonable that the increasing trend is attributed to the accumulation of charges. When the number is larger than 100, the bending feature seems to become more and more unclear with the increase of the measurement number. This can also be seen that, the snap-in forces are large when the numbers are 200, 300, and 400. Also, the adhesion forces are large when the numbers are between 200 and 400, as shown in Fig. 5(b). Therefore, the increasing and decreasing trends of the adhesion force are all related with the number of charges. When the tip touches and then jumps off the sample, the charges are generated on both surfaces, although with the anti-static copper bar placed above the tip. That means the charges are generated by contacting and eliminated by the ionized air (generated by the bar) at the same time. However, the separation distance between the tip and the sample is just so small that the ionized air is not as effective as it should be. This results in that the generation rate of charges is larger than the elimination rate at the beginning. This leads to that the electrostatic charges continue to accumulate at the beginning of the experiment. As time goes on, the number of charges begins to decrease, resulting in the decrease of the adhesion force in each level.

After analyzing the change trends of the adhesion force, we will discuss why the data of adhesion force are grouped into different clusters or levels. In the process of recording many force–displacement curves at a single

location, the surface topography of the sample contacting with the tip is likely to be changed for different measurements. For one thing, the contact when the tip snaps into contact with the sample is slightly different from that when the applied load is the maximum. As the cantilever bends upward, the tip will slip slightly in the direction parallel to the cantilever. For another, the vertical motion of the piezo cannot be entirely linear (due to creep, hysteresis, and aging, *etc.*). The stability is also dependent on the mechanical and electronic factors of the AFM (such as vibration, thermal drift, and noise, *etc.*). Therefore, during a series of measurements, the measured area of the sample should be larger than the area of the tip. That is another main reason we cannot get a constant adhesion at a single location.

The contact regions of the flat tip and sample are shown in Fig. 7. Circle A represents the ideal contact region which corresponds to the tip-sample contact area. Circle B represents the actual contact region which corresponds to the maximum area of interaction between the tip and sample. That is, the actual measurement range is larger than the end-face circle of the tip. The diameter of the end-face circle of the flat tip is ~1.73 μm, and the average peak-to-peak distance of the ridges of the grating is ~291 nm. If the tip is in contact with the sample entirely, the number of ridges in contact will be 5 or 6. As can be seen from Fig. 3, there are nanoscale irregularities on the sidewall or top of the ridges. The tip will touch the highest asperities on top of the ridges. There is an area just under the center of the end-face circle of the tip, shown by Circle C in Fig. 7. The tip will touch this area every time, since the nonlinear vertical motion of the scanner cannot be large. In this area, the electrostatic charges will continue to accumulate. However,

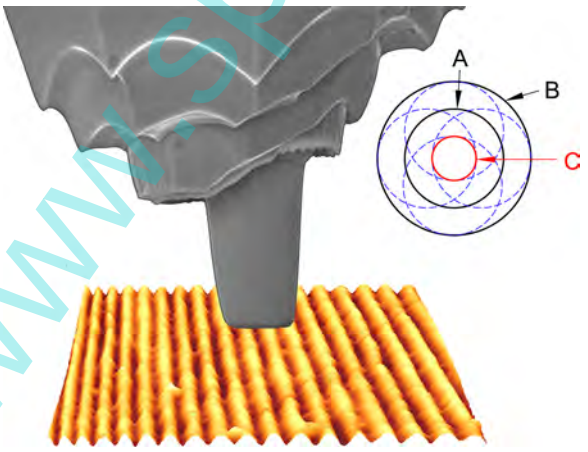

FIGURE 7 Contact regions of the flat tip and the sample. Circle A represents the ideal contact area which equals to the area of the circular end-face of the tip. Circle B represents the maximum contact area during the consecutive measurements at a single location. The dash lines circles represent the actual contact positions during measurements. Circle C represents the area where this tip will touch every time.

the electrostatic charges outside this area will only increase after touching by the tip.

There are some different positions on the sample surface contacting with the tip. The asperities are unchangeable for each position. Since there are different contact positions and the non-ideal contact, the adhesion forces are grouped into different levels. Moreover, the contact position is unpredictable. Therefore, the adhesion force will jump to other levels when the position is changed. When the current position is touched by the tip, the charges in this position will increase. As mentioned before, the charges will not dissipate or dissipate slowly, with a cumulative effect. Therefore, the charges in each position will increase gradually. There is an area (shown by Circle C in Fig. 7) where the charges will increase after each touch. Therefore, the adhesion forces in some levels shows to increase discontinuously.

Under ambient conditions, the relation of adhesion force and measurement number at a single location (Location 3) is shown in Fig. 8. The data of adhesion force are also grouped into several levels. However, the boundaries of the levels are not clear comparing with those in dry nitrogen. The feature of long-range electrostatic force was not found from the force–displacement curves. That is, there are only a few or no charges on the surfaces. The dominant contribution of adhesion is the capillary force.

Under ambient conditions, the capillary force is always present, and the vdW force is relatively small comparing with the capillary force. Generally speaking, there are two water transport mechanisms in the formation of water capillary bridges between the tip and the sample: (1) condensation of water vapor in the gap and (2) adsorption of water molecules on the surface region around the contact and flow of thin water film toward the growing meniscus [34–36]. Since both surfaces are hydrophilic, the liquid bridge formed is concave. Young–Laplace equation can be used to describe pressure difference Δp across the surface. It is $\Delta p = \gamma_L\left(r_1^{-1} + r_2^{-1}\right)$, where γ_L is the

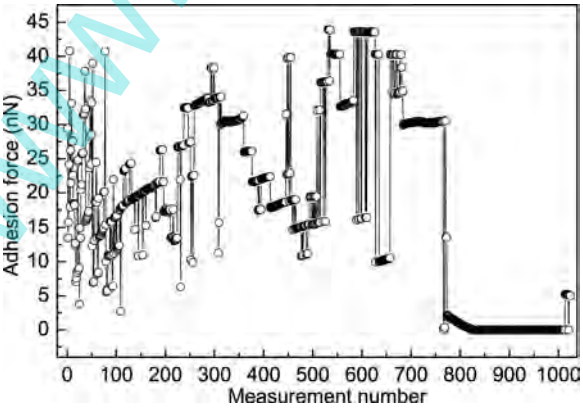

FIGURE 8 Adhesion forces versus sequential measurement number using the flat tip at Location 3 under ambient conditions.

surface tension or surface energy of the liquid film, r_1 are r_2 the principal radii of curvature of the surface. It can be seen that the pressure inside the liquid is smaller than the gas pressure for a concave meniscus. If the film outside the contact zone is flat, the pressure difference between the outside and inside of the interface is vanished. Therefore, the pressure inside the liquid of a concave meniscus is smaller than that of the surrounding water film. That means the surrounding water film will flow toward the growing meniscus. After multiple contacts, the water films near the measurement location become thicker by capillary condensation and the flow of a thin water film. That is, larger and/or more numerous liquid bridges will be formed with the increase of the measurement number. Also, this can be understood by the total contact time. The total contact time increases with the measurement number due to the consecutive contacts at a single location. Under high relative humidity, the adhesion force increases with the contact time [34]. This eventually leads to the increasing trend of the adhesion force in each level, when the number is lower than 550, as shown in Fig. 8.

However, this increasing trend is not maintained. When the number is larger than 550, the adhesion forces of some levels remain stable, while the other levels still show the increasing trend. In some positions, the size of the capillary meniscus and the number of water bridges may not increase after so many contacts. This leads to the stable adhesion force.

When the number reaches 773, the adhesion force jumps to a low value, and decreases with the measurement number. When the number is between 822 and 1014, the adhesion force remains nearly zero. Then the adhesion force jumps to ~5 nN for the last ten values. The low value (near zero) of the adhesion force is a very strange behavior. Figure 9 shows the retraction

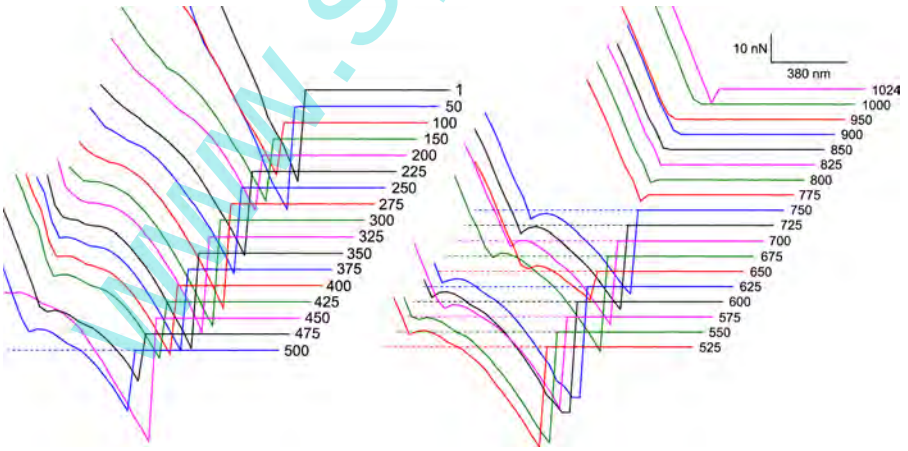

FIGURE 9 Lines of the retraction segments of force–displacement curves using the flat tip at Location 3 under ambient conditions. The dash lines are the prolongation of the zero lines. The measurement numbers are marked on the right side of the curves.

parts of force–displacement curves obtained using the flat tip at Location 3. Usually, the tip will be firmly contacted with the sample due to the adhesion with the retraction of the sample. The displacements of the tip and the sample are the same, leading to a straight contact line. This is true when the measurement numbers are 1–100 and 775–1024, as shown in Fig. 9. However, when the measurement number is between 150 and 750, the contact lines of the retraction curves are not straight lines. The curving feature becomes more and more clear with the increase of the measurement number. Also, this feature is above the zero line at first. When the measurement number is larger than 700, the feature is below zero lines. For the Curve 750 shown in Fig. 9, the most left segment is a straight line, and it crosses the prolongation of the zero line. That means the cantilever has bent downward. For some unknown reasons, the tip was pushed up suddenly, and then continued to run down with the sample until jumping off the sample. This strange behavior is shown when the measurement number is between ~420 and 772. After Curve 773, low adhesion forces are obtained. These measured low values may be the measurements of these features. We really have no certain explanation why the phenomenon happens. It may be related to a very particular contacting position.

From Figs. 5 and 8, the adhesion forces are all grouped into levels under different conditions. However, the adhesion behaviors in a single cluster are different. In order to compare and analyze the adhesion behavior under these conditions, three segments are selected from Figs. 5(a), 5(b), and 8, and are replotted in the same figure, as shown in Fig. 10. It can be observed that the fluctuation behaviors of these segments are different. Here, the fluctuation refers to the difference between two successive adhesion forces in a single cluster. In dry nitrogen, the adhesion force shows the middle fluctuation. In dry nitrogen, with static charges removal, the adhesion force shows

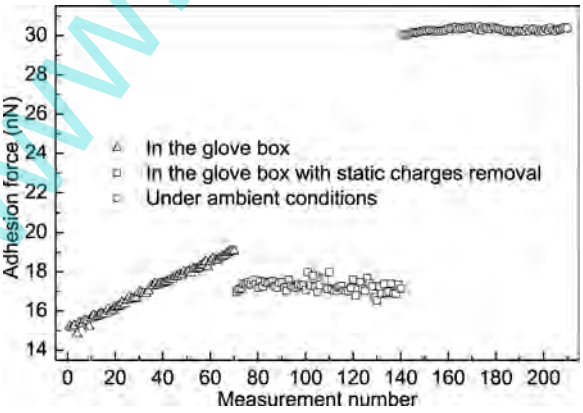

FIGURE 10 Adhesion force versus measurement number using the flat tip under three situations. These segments are selected from Figs. 5(a), 5(b), and 8.

the largest fluctuation. Under ambient conditions, the adhesion force shows the smallest fluctuation. The different fluctuation behaviors under three conditions may be attributed to the dominant interactions of the adhesion force. In dry nitrogen, the dominant interactions are the vdW force and electrostatic force. The accumulation of charges leads to the increase of adhesion with middle fluctuation. In dry nitrogen, with static charges removal, the charges are generated by contacting and eliminated by the ionized air at the same time. This leads to the largest fluctuation of adhesion force. Under ambient conditions, the size of capillary meniscus grows steadily by successive contacts, and this leads to the smallest fluctuation of adhesion force.

In dry nitrogen (without static charges removal) and under ambient conditions, the dominant contributions of adhesion are the electrostatic force and the capillary force, respectively. However, by using the flat tip, the adhesion forces in increasing, decreasing and stable trends are all observed under both conditions. The adhesion forces are all grouped into different clusters or levels in dry nitrogen, in dry nitrogen (with static charges removal) and under ambient conditions. The phenomenon does not depend on the environmental conditions, and should be attributed to the special structure of the sample and multi-asperity contact.

4. CONCLUSIONS

The outcomes show that the adhesion behavior at a single location depends largely on the contact geometry, surface topography, instrumental parameters, and the environment. Moreover, these factors are mutually coupled with each other to determine the final adhesion. A special surface structure will lead to special adhesion behaviors by repetitive measurements. The data of adhesion force are all grouped into several levels under ambient conditions and in dry nitrogen. In dry nitrogen (with static charge removal), the adhesion force in each level first increases and then decreases slightly. In dry nitrogen and under ambient conditions, the adhesion forces in different levels increase with the measurement number, and jump between different levels. The increase of adhesion force was ascribed to the accumulation of electrostatic charges and the increased size of the capillary meniscus, respectively. The flat tip cannot probe the grooves between the ridges to neutralize the charges there. This leads to the accumulation of charges in dry nitrogen. The electrostatic charges will be increased only after contact and separation and have an additive effect. When the charges are saturated, the adhesion behavior becomes stable. Under ambient conditions, the adhesion force will also be stable when the size of the capillary meniscus does not increase. However, the decreasing trend is also observed in dry nitrogen, which may be caused by the non-uniformity of charges or the polarity reversal due to material transfer. The decreasing trend and zero

adhesion forces are also observed under ambient conditions, the reason of which remains unknown.

By using the flat tip, the fluctuation behaviors of a single adhesion cluster under different conditions are different. This was attributed to the different dominant interactions of the adhesion force. In dry nitrogen, the accumulation of charges leads to the middle fluctuation. In dry nitrogen, with static charges removal, the charges are generated by contacting and eliminated by the ionized air at the same time. This leads to the largest fluctuation. Under ambient conditions, the size of capillary meniscus grows steadily by successive contacts, and this leads to the smallest fluctuation. Also, fluctuation behaviors are almost the same when the adhesion forces are in the decreasing trend and stable state.

FUNDING

The work was supported by the National Natural Science Foundation of China under Grant 51175182.

REFERENCES

[1] Zhao, Y. P., Wang, L. S., and Yu, T. X., *J. Adhes. Sci. Technol.* **17**, 519–546 (2003).
[2] Zaghloul, U., Papaioannou, G., Bhushan, B., Coccetti, F., Pons, P., and Plana, R., *Microelectron. Reliab.* **51**, 1810–1818 (2011).
[3] Butt, H. J., Cappella, B., and Kappl, M., *Surf. Sci. Rep.* **59**, 1–152 (2005).
[4] Fischer, H. R. and Gelinck, E. R. M., *Appl. Surf. Sci.* **258**, 9011–9017 (2012).
[5] Kappl, M. and Butt, H. J., *Part. Part. Syst. Char.* **19**, 129–143 (2002).
[6] Ando, Y., *Langmuir* **24**, 1418–1424 (2008).
[7] Ferreira, O. D. S., Gelinck, E., de Graaf, D., and Fischer, H., *Appl. Surf. Sci.* **257**, 48–55 (2010).
[8] Çolak, A., Wormeester, H., Zandvliet, H. J. W., and Poelsema, B., *Appl. Surf. Sci.* **258**, 6938–6942 (2012).
[9] You, S. and Wan, M. P., *Langmuir* **29**, 9104–9117 (2013).
[10] Awada, H., Noel, O., Hamieh, T., Kazzi, Y., and Brogly, M., *Thin Solid Films* **519**, 3690–3694 (2011).
[11] Yaqoob, M. A., de Rooij, M. B., and Schipper, D. J., *Tribol. Lett.* **49**, 491–499 (2013).
[12] Çolak, A., Wormeester, H., Zandvliet, H. J. W., and Poelsema, B., *Appl. Surf. Sci.* **308**, 106–112 (2014).
[13] Ibrahim, T. H., Burk, T. R., Etzler, F. M., and Neuman, R. D., *J. Adhes. Sci. Technol.* **14**, 1225–1242 (2000).
[14] Tormoen, G. W. and Drelich, J., *J. Adhes. Sci. Technol.* **19**, 181–198 (2005).
[15] Lai, T. and Huang, P., *Sci. China Technol. Sci.* **56**, 2934–2952 (2013).
[16] Hutter, J. L. and Bechhoefer, J., *Rev. Sci. Instrum.* **64**, 1868–1873 (1993).

[17] Van Oss, C. J., Chaudhury, M. K., and Good, R. J., *Chem. Rev.* **88**, 927–941 (1988).
[18] Van Oss, C. J., *Interfacial Forces in Aqueous Media*, (Taylor & Francis, New York, 2006).
[19] Izadi, H. and Penlidis, A., *Macromol. React. Eng.* **7**, 588–608 (2013).
[20] Lacks, D. J. and Sankaran, R. M., *J. Phys. D Appl. Phys.* **44**, 453001 (2011).
[21] Watson, P. K. and Yu, Z. Z., *J. Electrostat.* **40–41**, 67–72 (1997).
[22] Guerret-Piecourt, C., Bec, S., and Treheux, D., *C. R. Acad. Sci. Paris Série IV* **2**, 761–774 (2001).
[23] Burnham, N. A., Colton, R. J., and Pollock, H. M., *Nanotechnology* **4**, 64–80 (1993).
[24] Messina, R., *J. Chem. Phys.* **117**, 11062–11074 (2002).
[25] Khachatourian, A., Chan, H.-K., Stace, A. J., and Bichoutskaia, E., *J. Chem. Phys.* **140**, 074107 (2014).
[26] Horn, R. G. and Smith, D. T., *Science* **256**, 362–364 (1992).
[27] McGuiggan, P. M., *Langmuir* **24**, 3970–3976 (2008).
[28] Izadi, H., Zhao, B., Han, Y., McManus, N., and Penlidis, A., *J. Polym. Sci. Polym. Phys.* **50**, 846–851 (2012).
[29] Thomas III, S. W., Vella, S. L., Kaufman, G. K., and Whitesides, G. M., *Angew. Chem. Int. Ed.* **47**, 6654–6656 (2008).
[30] Castle, G. S. P. and Schein, L. B., *J. Electrostat.* **36**, 165–173 (1995).
[31] Baytekin, H. T., Patashinski, A. Z., Branicki, M., Baytekin, B., Soh, S., and Grzybowski, B. A., *Science* **333**, 308–312 (2011).
[32] Baytekin, H. T., Baytekin, B., Incorvati, J. T., and Grzybowski, B. A., *Angew. Chem.* **124**, 4927–4931 (2012).
[33] Lacks, D. J., *Angew. Chem. Int. Ed.* **51**, 6822–6823 (2012).
[34] Wei, Z. and Zhao, Y.-P., *J. Phys. D Appl. Phys.* **40**, 4368–4375 (2007).
[35] Rabinovich, Y. I., Singh, A., Hahn, M., Brown, S., and Moudgil, B., *Langmuir* **27**, 13514–13523 (2011).
[36] Sirghi, L., *Langmuir* **28**, 2558–2566 (2012).